De Novo Variants in *LMNB1* Cause Pronounced Syndromic Microcephaly and Disruption of Nuclear Envelope Integrity

Francesca Cristofoli,[1,12] Tonya Moss,[2,12] Hannah W. Moore,[3] Koen Devriendt,[1] Heather Flanagan-Steet,[2] Melanie May,[2] Julie Jones,[2] Filip Roelens,[4] Carmen Fons,[5] Anna Fernandez,[5] Loreto Martorell,[6] Angelo Selicorni,[7] Silvia Maitz,[8] Giuseppina Vitiello,[9] Gerd Van der Hoeven,[10] Steven A. Skinner,[3] Mathieu Bollen,[10] Joris R. Vermeesch,[1] Richard Steet,[2,*] and Hilde Van Esch[1,11,*]

Summary

Lamin B1 plays an important role in the nuclear envelope stability, the regulation of gene expression, and neural development. Duplication of *LMNB1*, or missense mutations increasing *LMNB1* expression, are associated with autosomal-dominant leukodystrophy. On the basis of its role in neurogenesis, it has been postulated that *LMNB1* variants could cause microcephaly. Here, we confirm this hypothesis with the identification of *de novo* mutations in *LMNB1* in seven individuals with pronounced primary microcephaly (ranging from −3.6 to −12 SD) associated with relative short stature and variable degree of intellectual disability and neurological features as the core symptoms. Simplified gyral pattern of the cortex and abnormal corpus callosum were noted on MRI of three individuals, and these individuals also presented with a more severe phenotype. Functional analysis of the three missense mutations showed impaired formation of the LMNB1 nuclear lamina. The two variants located within the head group of LMNB1 result in a decrease in the nuclear localization of the protein and an increase in misshapen nuclei. We further demonstrate that another mutation, located in the coil region, leads to increased frequency of condensed nuclei and lower steady-state levels of lamin B1 in proband lymphoblasts. Our findings collectively indicate that *de novo* mutations in *LMNB1* result in a dominant and damaging effect on nuclear envelope formation that correlates with microcephaly in humans. This adds *LMNB1* to the growing list of genes implicated in severe autosomal-dominant microcephaly and broadens the phenotypic spectrum of the laminopathies.

The nuclear lamina (NL) is a filamentous network of proteins lying beneath the inner nuclear membrane of most metazoan cells.[1] Although originally thought to be an inert structural scaffold for the nuclear envelope, several studies have demonstrated complex roles for the NL in cell metabolism. Besides contributing to the mechanical stability of the nuclear envelope, controlling the position of nuclear pore complexes, and anchoring and organizing the chromatin, the NL is involved in the regulation of DNA replication, transcription, and repair in cell cycle progression, nuclear migration, and apoptosis.[2–6] The major components of the NL are type V intermediate filament proteins grouped in two distinct classes, namely A- and B-type lamins. In mammals, A-type lamins (A, AΔ10, C, and C2) are generated by alternative splicing of a single locus (*LMNA* in humans [MIM: 150330]) and expressed primarily in a subset of differentiated cells but also at low abundance early in development. Conversely, B-type lamins are encoded by two distinct genes (*LMNB1* [MIM: 150340] and *LMNB2* [MIM:

150341] in humans) and expressed in almost all known cell types beginning at earliest stages of development.[3,7,8] Lamin-deficient mouse models have been used to elucidate their roles during development.[9–11] B-type lamin-deficient mice are neonatal lethal and display characteristic brain abnormalities that point to an essential role for B-type lamins in proper organogenesis as well as in neuronal migration and patterning during brain development. Both LMNB1- and LMNB2-deficient mice—either conventional or forebrain-specific—display neuronal migration and cortical layering defects. In both animal models, the cellularity of the forebrain is markedly reduced, suggesting compromised survival of neurons. These defects are probably due to a weakened NL that interferes with proper nucleokinesis, the nuclear translocation process required for neuronal migration during corticogenesis, resulting in turn in nuclear membrane ruptures that result in interspersion of nuclear and cytoplasmic contents and ultimately cell death.[11] Lamin B-deficient neurons are characterized by aberrant

nuclear morphology, abnormal spindle orientation, cell cycle defects, and asymmetric distribution of other nuclear membrane components.[9,12–17] LMNB1 is specifically required for dendritic development in primary mouse cortical neurons,[18] proper differentiation of murine neural stem cells into neurons and astroglial-like cells,[19] and the formation of functional olfactory sensory neurons.[20] On the basis of these *in vitro* and animal data, it has been anticipated that *LMNB1* mutations may contribute to microcephaly in humans.[13–15,21]

In humans, duplication of *LMNB1* causes adult-onset autosomal-dominant leukodystrophy (ADLD [MIM: 169500]).[22] More recently, an individual with a *de novo* c.85C>T (p.Arg29Trp) *LMNB1* variant presenting with cerebellar ataxia and vanishing white matter disease of the cerebellum has been described.[23] Here, we describe seven individuals with novel variants in *LMNB1*, all presenting with pronounced primary microcephaly (ranging from −3.6 to −12 SD) associated with relative short stature and a variable degree of intellectual disability as the core symptoms (Figure 1); these individuals were from five different families. In three individuals, simplified gyral pattern of the cortex and abnormal corpus callosum were noted on MRI (Figure 1). These individuals also showed a more severe neurological phenotype with severe feeding difficulties, spasticity, epilepsy, and neurogenic scoliosis. Individuals 1 and 2 were diagnosed as part of a research project on syndromic microcephaly. Individuals 3–7 were identified and recruited via GeneMatcher.[24] An overview of the clinical features present in the affected individuals is presented in Table 1. More detailed clinical descriptions are provided in the Supplemental Notes.

All studies were approved by the respective ethical committees of the collaborating institutions and performed on genomic DNA extracted from the index and the parents. The parents of subjects provided consent for genetic studies and publication of photographs shown in this study. The various mutations were identified via trio whole-exome sequencing (WES; individuals 1, 3, and 4) or by custom-designed gene panel (individuals 5–7), and technical details are provided in Table S1. In individual 1, a *de novo* missense mutation, c.455C>G, in exon 2 of *LMNB1* (GenBank: NM_005573.3; MIM: 150340) was identified, leading to a p. Ala152Gly change (NP_005564.1). Individuals 3 and 4 each carry a *de novo* mutation, c.97A>G and c.124C>T resulting in p.Lys33Glu and p.Arg42Trp, respectively, in exon 1 of *LMNB1* (Table 1). The location of the mutations is shown in Figure 2A, and all three residues are highly conserved and predicted to be deleterious by various *in silico* methods (Table S2). Individuals 5, 6, and 7 belong to an Arabic sibship, and trio WES identified the same splice mutation, c.939+1G>A, in all three affected children. Further analysis confirmed mosaicism for the c.939+1G>A mutation (15%) in the blood of the father. Human Splicing Finder v.3.1 predicts that this variant disrupts the exon 5 consensus donor splice site, which might result in exon skipping. However, the mutation could also uncover a neighboring exonic or intronic cryptic splice site.[25] *In silico* prediction via the NNSplice[26] and the Alternative Splice Site Predictor[27] software tools indeed revealed a weaker

Table 1. Overview of Clinical Features

	Individual 1	Individual 2	Individual 3	Individual 4	Individual 5	Individual 6	Individual 7
LMNB1 (NM_005573.3) genomic variation GRCh37	exon2: c.455C>G	5q23.2(126,1 49,952-126,159, 137)x1mat	exon1: c.97A>G	exon 1: c.124C>T	c.939+1G>A splice variant		
Protein change	p.Ala152Gly	in-frame p.Ser314_Thr497del	p.Lys33Glu	p.Arg42Trp	elongation of exon 5, introducing 6 novel amino acids?		
Inheritance	*de novo*	maternal	*de novo*	*de novo*	father 15% mosaic for the mutation		
Gender	m	f	f	f	f	m	m
Ethnicity	Caucasian	Caucasian	Caucasian	Caucasian	Arabic	Arabic	Arabic

Birth Parameters

	Individual 1	Individual 2	Individual 3	Individual 4	Individual 5	Individual 6	Individual 7
OFC at birth	25 cm, term	32 cm, term	28 cm, preterm 35 weeks	29 cm, term	N/A	28.5 cm, term	27.5 cm, term
Length at birth	46 cm	51 cm	42 cm	48.9 cm	N/A	N/A	48 cm
Weight at birth	2610 g	3460 g	2190 g	2890 g	N/A	2500 g	2700 g
Growth latest assessment	9 years 6 months	6 years	5 years 7 months	2 years 8 months	1 year 8 months	11 years 11 months	10 years 6 months
Length	122 cm (−2.7 SD)	119.5 cm (+0.7 SD)	92 cm (−4.8 SD)	81 cm (−2.6 SD)	77 cm (−2.4 SD)	122 cm (−4 SD)	125.34 cm (−2.5 SD)
OFC	42 cm (−6.8 SD)	45.1 cm (−3.6 SD)	36.5 cm (−12 SD)	36.1 cm (−12 SD)	35 cm (−4.4 SD)	40 cm (−10 SD)	39 cm (−10 SD)

Facial Features

	Individual 1	Individual 2	Individual 3	Individual 4	Individual 5	Individual 6	Individual 7
Facial dysmorphism	no	pronounced and long philtrum, short nose, trigonocephaly	prominent nasal root, protruding tongue	fullness glabellar region, bitemporal narrowing, prominent eyes and eyelashes, upslanting palpebral fissures	no	gingival hypertrophy	gingival hypertrophy

Neurological

	Individual 1	Individual 2	Individual 3	Individual 4	Individual 5	Individual 6	Individual 7
Degree of DD/ID	moderate to severe	mild	severe	significant developmental delay	significant developmental delay	severe	severe
Brain imaging (MRI)	small brain, normal structures	small brain, normal structures	pachygyria, thin corpus callosum	simplified gyral pattern, dysgenesis of corpus callosum	N/A	simplified gyral pattern, dysgenesis of the corpus callosum	simplified gyral pattern
Neurological abnormalities	no	no	spasticity limbs, inability to walk	seizures (controlled)	seizures (controlled), hypotonia	seizures (controlled), severe axial hypotonia, spastic tetraparesis, no language or communication	seizures (controlled), severe axial hypotonia, spastic tetraparesis, no language or communication
Visual impairment	no	no	no	suspected cortical visual impairment	N/A	cortical visual impairment	cortical visual impairment
Skeletal abnormalities	no	no	scoliosis	no	mild scoliosis	severe scoliosis	severe scoliosis
Gastro-intestinal abnormalities	feeding difficulties	no	feeding difficulties	feeding difficulties, G-tube	no	feeding difficulties, G-tube	feeding difficulties, G-tube
Other	none	OFC mother 50.5 cm (−2.5 SD), low educational level, long philtrum	patent foramen ovale	recurrent pneumonia	none	recurrent pneumonia	recurrent pneumonia

Table 1. Continued

	Individual 1	Individual 2	Individual 3	Individual 4	Individual 5	Individual 6	Individual 7
Chromosomal microarray	normal (OGT Cytosure)	intragenic *LMNB1* deletion (OGT Cytosure)	normal (Agilent 180k Hg19)	15q25.3(85,811,682- 86,140,453)x3 pat (VOUS; CytoScan DX)	N/A	17p13.3 (954,760- 1,235,739)x3 (VOUS; CMA-ISCA)	normal

m, male; f, female; N/A, not assessed; OFC, occipitofrontal circumference; VOUS, variant of unknown significance.

cryptic donor splice sequence 18 nucleotides downstream of the canonical site, which could result in a partial intronic retention and extension of exon 5 by six novel amino acids (Figure 2B). Unfortunately, we were unable to test this hypothesis because the family was unavailable for further RNA studies. None of the above identified variants is present in the dbSNP, 1000 Genomes, Leiden Open Variation Database (LOVD) 3.1, NHLBI Exome Sequencing Project (ESP), or gnomAD databases. Variants have been deposited in ClinVar and have the accession numbers SCV001296959–SCV001296963.

In individual 2, an intragenic heterozygous *LMNB1* deletion was identified by chromosomal microarrays (OGT Cytosure 180k, v3 array). This deletion was inherited from an equally affected mother in whom it occurred *de novo*. The phenotype in individual 2 is milder with a head circumference at −3.6 SD and mild-to-borderline cognitive deficit compared to the other individuals. The deletion spans exons 6–8 of the gene, resulting in a 552-amino-acids in-frame deletion (p.Ser314_Thr497), possibly resulting in a shorter version of the protein noticeably lacking the nuclear localization signal (NLS) (Figure 2). To our knowledge, no other intragenic deletion only affecting *LMNB1* has been reported in any of the large CNV databases (Decipher, Ensembl Genome Browser). On the contrary, several individuals with large contiguous gene deletions on chromosome 5q23.2, including deletion of *LMNB1,* have been reported and only in one affected individual, harboring a 134 Mb deletion, microcephaly was noted (Decipher ID: 282760). This argues against haploinsufficiency as a potential mechanism for the phenotypes in this cohort because *LMNB1* seems to be tolerant to loss of function (pLI score 0.55). Therefore, we predict that a dominant-negative effect of the different *de novo* mutations is more likely.

To investigate the functional significance of the identified *LMNB1* variants, we introduced cDNAs coding for the different missense changes into a *LMNB1*-null HeLa cell line and analyzed the ability of these variant lamin B1 molecules to form an NL. Two variants (p.Lys33Glu and p.Arg42Trp) lie within or proximal to the head domain of the protein, whereas p.Ala152Gly resides within the first coil domain (coil 1B, Figure 2A). Biochemical validation of the *LMNB1*-null HeLa cell line demonstrated complete loss of lamin B1 but no change in the amount of lamin A/C as gauged by immunoblot (Figure 3A). Immunofluorescent staining of both lamin B1 and lamin A/C confirmed the absence of lamin B1 and also showed that the NL formed

by lamin A/C and overall nuclear morphology is not obviously altered in the null line (Figure 3B). We performed transfection of *LMNB1* variant cDNAs into *LMNB1*-null HeLa cells followed by immunoblot analysis to look at the amount and mobility of lamin B1 (Figures 3C and 3D). In all cases, the transfection led to a significant increase (∼10- to 15-fold) in overall lamin B1 and there were no differences in the corresponding steady-state level of lamin A/C. Lamin B1 ran as a single band at 65 kDa, slightly higher than the faint lamin B1 detected in the parental HeLa cell line. A consistent reduction in steady-state level of p.Ala152Gly lamin B1 was observed despite the introduction of equivalent cDNA amount, suggesting the possible instability of this lamin B1 variant (Figure 3E).

We then performed immunofluorescence staining on the transfected *LMNB1*-null cells to evaluate whether the missense variants alter the formation of the lamin B1 NL (Figure 4). Quantification revealed a much higher abundance of cells with an abnormal nuclear lamina percentage when any of the three missense variants were expressed compared to the wild type (WT). Both the p.Lys33Glu and p.Arg42Trp lamina also appeared diffuse and poorly formed: there was no discrete boundary and dispersion of lamin B1 throughout the cell. In many cells with an abnormal lamina, aggregates of lamin B1 were observed. The lamin A/C NL was variably affected in these transfected cells. An altered morphology of the lamin B1 lamina was noted in cells transfected with the p.Ala152Gly-encoding cDNA, but there was not the same loss of boundary and diffusion seen with the other two variants. The lamin A/C NL in the p.Ala152Gly-transfected cells was ruffled and irregular, suggestive of a more global disruption of the envelope (Figure 4A). In light of lamin B1's established role in the maintenance of nuclear morphology, we also analyzed the morphology of the nucleus in the transfected cells, observing a significant increase in the number of cells with a bi-/multi-lobed phenotype with both p.Lys33Glu- and p.Arg42Trp-encoding cDNA (Figure 4B). These data support the idea that the NL is disrupted when these variant lamin B1 proteins are present, resulting in a misshapen and irregular nuclear structure. This increase was less pronounced in the HeLa cells transfected with cDNA encoding p.Ala152Gly; these cells instead showed an increase in the percentage of cells with condensed nuclei. These condensed and often smaller nuclei were noted at lower frequency in the other transfected cells and may arise as a result of overexpression.
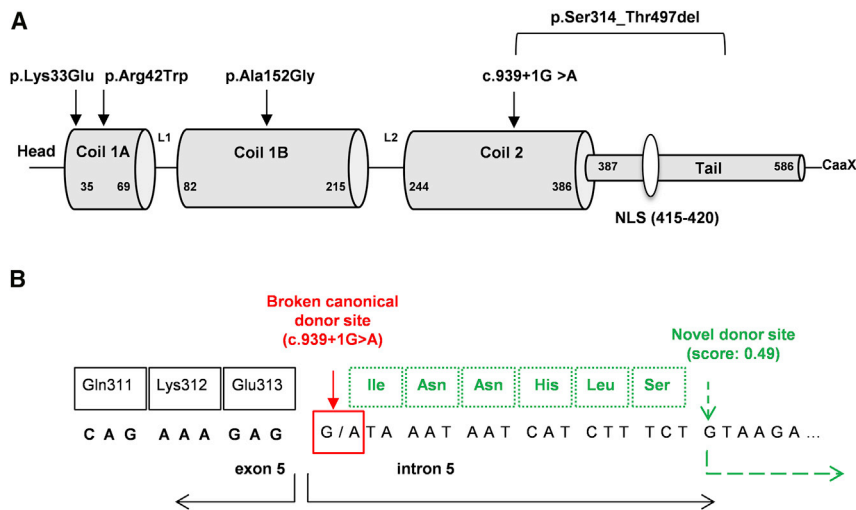
The diffuse NL observed in cells transfected with the p.Lys33Glu- and p.Arg42Trp-encoding cDNA indicated that these variants may impact the head domain of the protein and prevent proper formation of the lamina network. To address this hypothesis, we performed subcellular fractionation on transfected cells and the resulting nuclear and cytosolic fractions were analyzed by immunoblot (Figure 5). When analyzing the nuclear fraction only, a substantial reduction in the amount of lamin B1 recovered in the nuclear fraction of both the p.Lys33Glu- and p.Arg42Trp-transfected cell populations was observed (Figure 5A). The amount of nuclear lamin B1 recovered from the p.Ala152Gly-transfected cell population was also lower, possibly reflecting the overall decrease in steady-state levels of the variant form. The nuclear and cytosolic fractions were next analyzed in cells transfected with WT-, p.Lys33Glu-, p.Arg42Trp-, and p.Lys33Thr-encoding cDNA. The latter, p.Lys33Thr (c.98A>G), is a rare polymorphic variant (rs1303994586) that has been reported in gnomAD exomes with an allele frequency of 0.000008 (1/131,322 alleles), and so it served as a useful control for the specificity of the effects of the p.Lys33Glu variant. p.Lys33Glu- and p.Arg42Trp-transfected cells, but not p.Lys33Thr-transfected cells, again showed a clear decrease in amount of lamin B1 within the nuclear fraction, along with a corresponding increase in lamin B1 within the cytosol fraction (Figure 5B), when compared to WT. Subsequent immunoblotting with lamin A/C and GAPDH antibodies
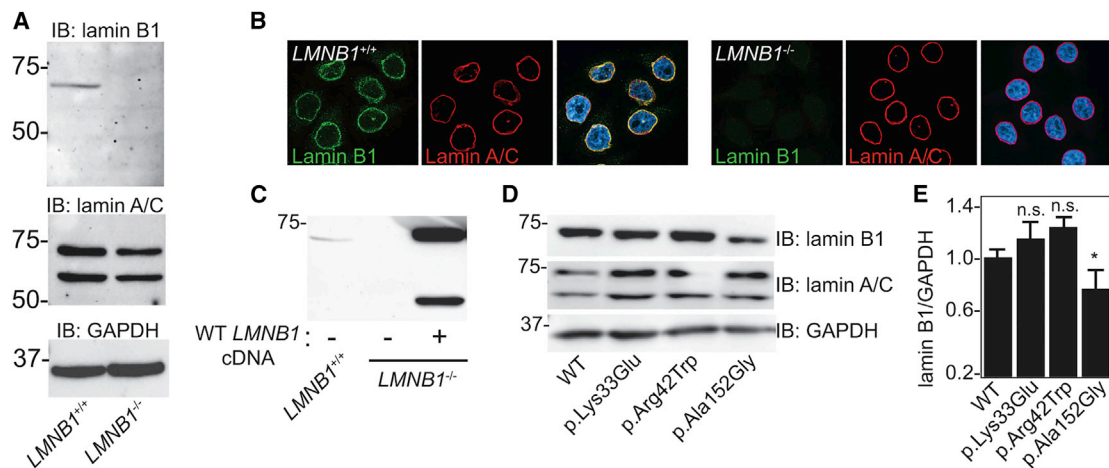

Figure 3. Validation of an *LMNB1*-Null HeLa Cell Line for Functional Characterization of *LMNB1* Variants

(A) Immunoblot analysis of lamin B1 and lamin A/C in parental (*LMNB1*$^{+/+}$) and *LMNB1*$^{-/-}$ HeLa cells. GAPDH was used to normalize protein loading.

(B) Immunostaining of lamin B1 (green) and lamin A/C (red) in HeLa cells. DAPI (blue) staining of the nucleus is shown in the merged images.

(C) Transfection of cDNA encoding WT *LMNB1* in the *LMNB1*$^{-/-}$ HeLa cells greatly increases the abundance of lamin B1 relative to *LMNB1*$^{+/+}$ HeLa cells.

(D) Expression of WT and variant-encoding cDNA in the *LMNB1*$^{-/-}$ HeLa cells followed by immunoblot analysis of whole-cell lysates.

(E) Quantification of the abundance of lamin B1 (relative to GAPDH) by densitometry in transfected HeLa cells (n = 4); *p ≤ 0.05.
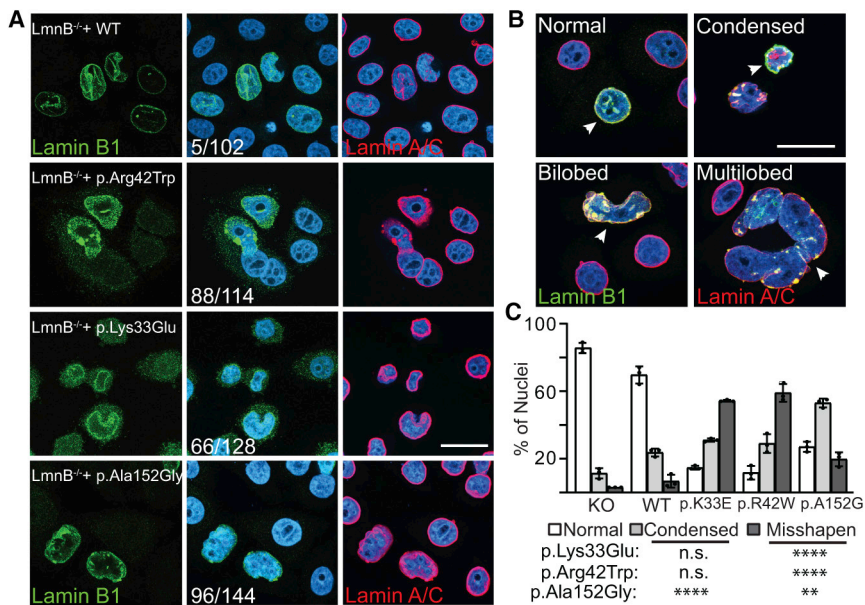
Figure 4. Introduction of Variant-Bearing *LMNB1* cDNAs Disrupts Nuclear Envelope Integrity

(A) Immunostaining of *LMNB1*$^{-/-}$ HeLa cells transfected with WT and variant-bearing *LMNB1* cDNAs (lamin B1, green; lamin A/C, red; DAPI, blue). The number of transfected cells with abnormal nuclear envelope morphology (versus the total cell quantified across at least four different fields from three independent staining experiments) is denoted in the middle panels. Scale bar represents 10 μm.

(B) Representative nuclear phenotypes observed in the transfected HeLa cells that were scored (the condensed phenotype was taken from the p.Ala152Gly cells and the bi-/multi-lobed phenotype was taken from the p.Lys33Glu cells); scale bar represents 10 μm.

(C) Quantification of the percentage of nuclei with a given phenotype from at least 100 cells scored across the three independent staining experiments; statistical analysis done with a Dunnett's test; **p ≤ 0.01, ****p ≤ 0.0001.

demonstrated the fidelity of the subcellular fractionation. Quantification by densitometry of four independent experiments showed a 73 ± 10% and 65 ± 6% decrease in nuclear lamin B1 in the p.Lys33Glu- and p.Arg42Trp-transfected cells, respectively. A modest reduction in the amount of p.Lys33Thr lamin B1 from the nuclear fraction was noted, but there was no detectable lamin B1 in the cytosolic fraction (Figure 5D). Collectively, these findings indicate that p.Lys33Glu and p.Arg42Trp behave in a similar manner and result in improper formation of an NL when introduced alone in the *LMNB1*-null HeLa cells. Their increased abundance within the cytosolic fraction further suggests that the solubility of the lamin B1 monomers within this compartment increases when they fail to incorporate into the laminar network.

Next, we compared the impact of the LMNB1 p.Arg29Trp variant, recently reported in an individual with leukodystrophy and cerebellar involvement,
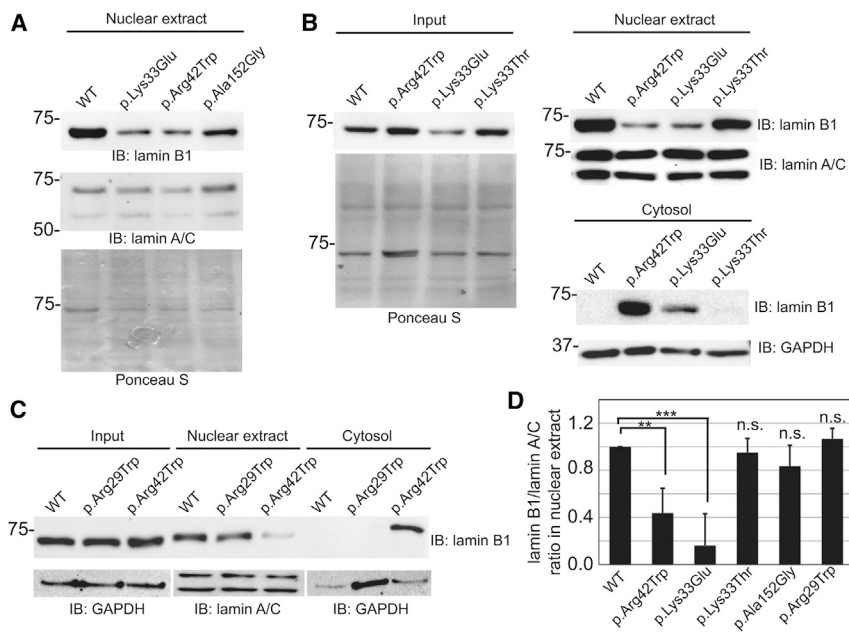

Figure 5. Increased Partitioning of p.Lys33Glu and p.Arg42Trp Lamin B1 into the Cytosol

(A) Immunoblot analysis of lamin B1 and lamin A/C in nuclear extracts from *LMNB1*$^{-/-}$ HeLa cells transfected with WT and variant-bearing *LMNB1* cDNAs (n = 4). Ponceau S staining is shown as a loading control.

(B) Immunoblot analysis of lamin B1 in whole-cell lysates of *LMNB1*$^{-/-}$ HeLa cells transfected with WT and variant-bearing *LMNB1* cDNAs. The same transfected cells were subjected to subcellular fractionation to isolate nuclei and cytosol. These fractions were resolved by SDS-PAGE and analyzed by immunoblot. Representative images from four independent experiments are shown.

(C) Immunoblot analysis of *LMNB1*$^{-/-}$ HeLa whole-cell lysates and nuclear and cytosolic fractions from these cells following transfection with WT-, p.Arg29Trp-, and p.Arg42Trp-encoding cDNAs. GAPDH and lamin A/C blots are shown below (n = 3).

(D) Collective quantification by densitometry of the ratio of lamin B1 to lamin A/C in nuclear extracts shown in (A)–(C). Values were normalized to the ratio observed with WT *LMNB1* cDNA (ratio was set at 1.0 for each condition). Error bars denote standard deviation of the mean; p values were determined via Student's t test (**p < 0.01; ***p < 0.001).
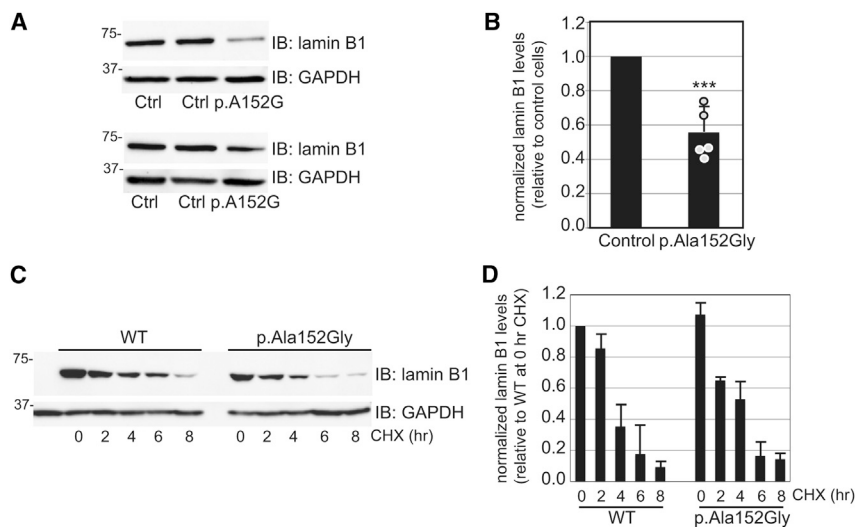
Figure 6. Reduced Steady-State Level of Lamin B1 in p.Ala152Gly Lymphoblasts

(A) Immunoblot analysis of lamin B1 in control and affected individual (p.Ala152Gly) lymphoblastoid cell lines. Representative results from two out of five independent experiments are shown.

(B) Quantification of the steady-state level of lamin B1 by densitometry and normalization to GAPDH levels (n = 5; statistical analysis performed via Student's t test; ***p < 0.001).

(C) $LMNB1^{-/-}$ HeLa cells transfected with WT- and p.Ala152Gly-encoding cDNAs were treated with cycloheximide for various times following lysis and analysis by SDS-PAGE and immunoblot. A representative blot from three independent experiments is shown.

(D) Quantification of lamin B relative to GAPDH (normalized to the WT 0 h cycloheximide treatment) from the three experiments is shown. Error bars represent standard deviations of the mean. No statistically significant differences in abundance were noted.

alongside the p.Arg42Trp variant by using the same experiment as above to evaluate whether these variants can be distinguished from each other with this assay. The results shown in Figure 5C (and quantified in Figure 5D) clearly demonstrate that only p.Arg42Trp leads to loss of integrity of the lamin B1 NL. This finding supports the notion that the p.Arg29Trp substitution is probably functionally distinct, resulting in a phenotype different from what is observed in the present cases.

Next, we sought to more clearly define the impact of the p.Ala152Gly variant and its mechanism of action and to confirm its effect on the steady-state level of lamin B1. Parallel sets of control and p.Ala152Gly proband-derived lymphoblasts were subjected to immunoblot analysis (Figure 6A) and the abundance of lamin B1 was quantified by densitometry (Figure 6B). As noted when the p.Ala152Gly variant encoding cDNA was introduced into the *LMNB1*-null HeLa cells, a decrease (56 ± 15% of control) in the steady-state level of lamin B1 was also observed in the proband lymphoblastoid cell lines (LCLs). This finding supports the instability of this variant lamin B1. In light of the fact that the individual has one normal *LMNB1* allele, it is possible that the variant form of the protein is degraded rapidly. We explored this mechanism in greater depth by treating *LMNB1*-null HeLa cells transfected with either WT- or p.Ala152Gly-encoding cDNA with cycloheximide to stop new protein translation and monitoring the loss of lamin B1 by immunoblot over time (Figure 6C). Although suggestive of enhanced turnover, quantification of three independent experiments failed to show a significant increase in the turnover of p.Ala152Gly compared to WT (Figure 6D).

Finally, the pronounced microcephaly and growth restriction seen in the individuals, together with the established role of lamin B1 in mitotic spindle formation, might point toward a spindle and/or mitotic defect underlying the microcephaly.[9,10,28] Using three proband-derived and two parental-control LCLs, we first analyzed the morphology of the nucleus in these cells, observing a significant increase in the number of cells with a bi-/multi-lobed phenotype in the p.Lys33Glu and p.Arg42Trp LCLs, confirming the observations in our HeLa system (Figure 7A). However, as shown in Figures 7B and 7C, the abnormal nuclear shape does not correlate with abnormal ploidy or failed mitotic segregation. In addition, we could not observe abnormal metaphase spindle formation in the proband LCLs compared to their parental controls.

In summary, we describe seven individuals presenting with severe microcephaly associated with cognitive deficit and neurological symptoms from five different families. Functional characterization of the three different missense variants demonstrated that these variants appear to disrupt the lamin B1 nuclear envelope when introduced into *LMNB1*-null HeLa cells, and there were variable effects on the lamin A/C NL. The two variants (p.Lys33Glu and p.Arg42Trp) that reside in the head region of the protein result in greatly increased recovery from the cytosol following subcellular fractionation, highlighting the importance of this domain in the formation of a stable, nuclear-localized laminar network. We speculate that mutation of lysine 33 is functionally relevant on a molecular level because this residue may be subject to acetylation as a regulatory mechanism. Although not a consensus site for any known post-translational modifications, the p.Arg42Trp variant might indirectly alter the modification of nearby phosphorylation or O-GlcNAc sites.

The p.Ala152Gly change did not result in increased cytosolic localization following subcellular fractionation, but this variant did disrupt nuclear envelope integrity when

A

B

FISH analysis with combination probes for chromosomes 13 and 21

	total nuclei scored	haploid	diploid	triploid	tetraploid
p.Ala152Gly proband	100	1	97	0	2
p.Arg42Trp proband	100	0	100	0	0
p.Lys33Glu proband	100	1	96	2	1
p.Lys33Glu parent	100	0	98	1	1
p.Arg42Trp parent	100	2	94	3	1

FISH analysis with combination probes for chromosomes X and Y

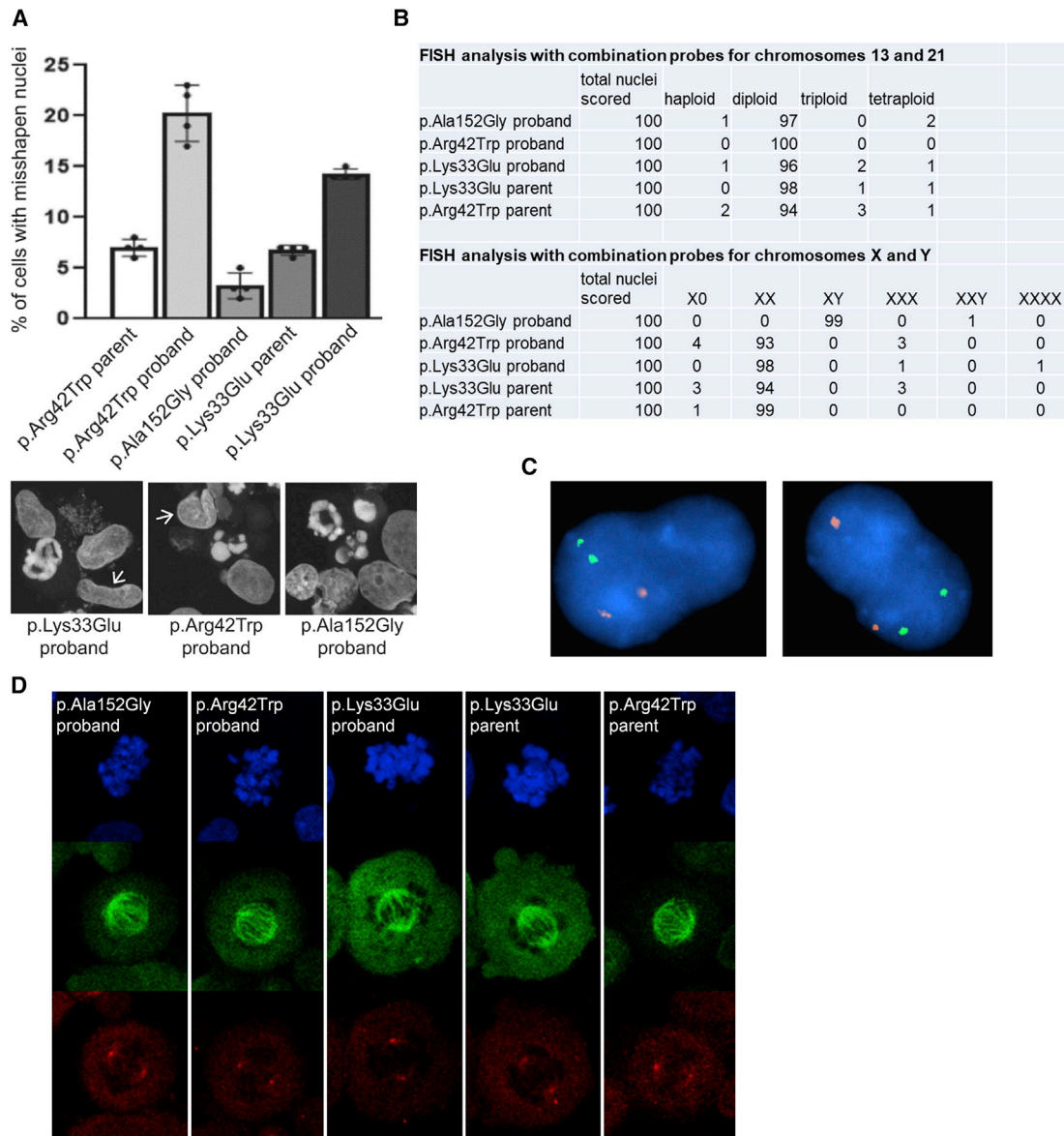|	total nuclei scored	X0	XX	XY	XXX	XXY	XXXX
p.Ala152Gly proband	100	0	0	99	0	1	0
p.Arg42Trp proband	100	4	93	0	3	0	0
p.Lys33Glu proband	100	0	98	0	1	0	1
p.Lys33Glu parent	100	3	94	0	3	0	0
p.Arg42Trp parent	100	1	99	0	0	0	0

C

D

Figure 7. Abnormal Nuclear Shape in Proband-Derived Lymphoblast Cells Does Not Correlate with Abnormal Mitotic Spindle Formation or Ploidy Alteration

(A) Quantification of the percentage of nuclei with a misshapen phenotype from at least 100 proband-derived lymphoblast cells scored across three independent staining experiments and compared to control-parent-derived lymphoblast cells. Representative images of DAPI-stained nuclei from the different LCL populations are shown below the graph. Arrows indicate the misshapen nuclei. Note condensed nuclei in the p.Ala152Gly LCL.

(B) Overview of ploidy screening results in 100 nuclei per LCL via two different fluorescence *in situ* hybridization (FISH) probe mixtures showing no difference between proband and parental control lines.

(C) Representative image of interphase FISH analysis with chromosomes 13/21 probe mixture showing normal diploid bi-lobed nuclei.

(D) Representative images of normal metaphase spindles stained with antibodies against α-tubulin (green) and γ-tubulin (red). At least 20 spindles were scored per LCL and no difference in morphology could be noted between proband and parental control cells.

introduced into the *LMNB1*-null HeLa cells. Localized to one of the coil domains, it is possible that this variant alters the conformation of lamin B1 in a way that weakens the NL. In addition, unlike the other variants, p.Ala152Gly seemed to have a more pronounced effect on the integrity of the lamin A/C envelope, which may indicate it alters nuclear envelope structure more globally. In the two other families, which include individuals 2 and 5–7 with the intragenic p.Ser314_Thr497 deletion and the splice mutation c.939+1G>A, respectively, we hypothesize an equally dominant-negative effect of the resulting abnormal lamin B1. The p.Ser314_Thr497 deletion affects the NLS, and one could again foresee insufficient protein abundance in the nucleus to form a stable laminar network.

In human neurons, where lamin B1 is more abundant, impaired nuclear envelope integrity can result in a spectrum of negative consequences that ultimately lead to microcephaly in affected individuals. As already shown

by the work of the Young SG lab, cortical neurons in lamin-B1-deficient mice show abnormal migration resulting in abnormal cortical layering, a phenotype similar to the simplified gyration seen on MRI in our affected individuals.[13,14] In addition, the same group more recently showed that absence of lamin B1 results in a weakened nuclear envelope, impairing nucleokinesis and leading to reduced neuronal survival.[11] Disruption of nuclear envelope integrity, as observed for the different variants, might not only interfere with the disassembly and assembly on the lamina during cell division, but also impact the survival and migration of neural precursors and hence lead to severe reduction of brain size. In addition, the role of lamin B1 in mitotic spindle formation might also point toward a spindle and/or mitotic defect underlying the microcephaly. Although we could not confirm this in the different proband lymphoblastoid cells, we cannot exclude this pathomechanism in other cell types, including neurons. Finally, alterations in the expression of genes that drive neurogenesis can arise in neuronal cells when contacts between the NL and chromatin are lost.[10]

In light of the multiple domains within the *LMNB1* gene product, it is feasible that different missense variants will impact lamin B1 function by unique mechanisms, and thus, case-by-case functional analysis is warranted. The present work also adds *LMNB1* to the growing list of genes implicated in severe autosomal-dominant microcephaly.

Data and Code Availability

All variants described in the study have been deposited in ClinVar: accession numbers SCV001296959–SCV001296963.

Supplemental Data

Supplemental Data can be found online at https://doi.org/10.1016/j.ajhg.2020.08.015.

Web Resources

Alternative Splice Site Predictor (ASSP), http://wangcomputing.com/assp/

ClinVar, https://www.ncbi.nlm.nih.gov/clinvar/

dbSNP, https://www.ncbi.nlm.nih.gov/snp/

Decipher, https://decipher.sanger.ac.uk/

Ensembl, http://www.ensembl.org/index.html

Genic intolerance, http://genic-intolerance.org/index.jsp

gnomAd, https://gnomad.broadinstitute.org/

HLBI Exome Sequencing Project (ESP) Exome Variant Server, https://evs.gs.washington.edu/EVS/

Human Splicing Finder 3.1, https://www.genomnis.com/access-hsf

Leiden Open Variation Database v.3.0, https://www.lovd.nl/

MutationTaster, http://mutationtaster.org/

NNSplice v.0.9, https://www.fruitfly.org/seq_tools/splice.html

OMIM, https://www.omim.org/

PolyPhen2, http://genetics.bwh.harvard.edu/pph2/

Provean (protein variation effect analyzer), http://provean.jcvi.org/index.php

References

1. Worman, H.J. (2012). Nuclear lamins and laminopathies. J. Pathol. *226*, 316–325.
2. Dechat, T., Pfleghaar, K., Sengupta, K., Shimi, T., Shumaker, D.K., Solimando, L., and Goldman, R.D. (2008). Nuclear lamins: major factors in the structural organization and function of the nucleus and chromatin. Genes Dev. *22*, 832–853.
3. Burke, B., and Stewart, C.L. (2013). The nuclear lamins: flexibility in function. Nat. Rev. Mol. Cell Biol. *14*, 13–24.
4. Davidson, P.M., and Lammerding, J. (2014). Broken nuclei–lamins, nuclear mechanics, and disease. Trends Cell Biol. *24*, 247–256.
5. Pascual-Reguant, L., Blanco, E., Galan, S., Le Dily, F., Cuartero, Y., Serra-Bardenys, G., Di Carlo, V., Iturbide, A., Cebrià-Costa, J.P., Nonell, L., et al. (2018). Lamin B1 mapping reveals the existence of dynamic and functional euchromatin lamin B1 domains. Nat. Commun. *9*, 3420.
6. Hah, J., and Kim, D.-H. (2019). Deciphering Nuclear Mechanobiology in Laminopathy. Cells *8*, 231.
7. Stewart, C., and Burke, B. (1987). Teratocarcinoma stem cells and early mouse embryos contain only a single major lamin polypeptide closely resembling lamin B. Cell *51*, 383–392.
8. Röber, R.A., Weber, K., and Osborn, M. (1989). Differential timing of nuclear lamin A/C expression in the various organs of the mouse embryo and the young animal: a developmental study. Development *105*, 365–378.
9. Vergnes, L., Péterfy, M., Bergo, M.O., Young, S.G., and Reue, K. (2004). Lamin B1 is required for mouse development and nuclear integrity. Proc. Natl. Acad. Sci. USA *101*, 10428–10433.
10. Kim, Y., Sharov, A.A., McDole, K., Cheng, M., Hao, H., Fan, C.-M., Gaiano, N., Ko, M.S.H., and Zheng, Y. (2011). Mouse B-type lamins are required for proper organogenesis but not by embryonic stem cells. Science *334*, 1706–1710.
11. Chen, N.Y., Yang, Y., Weston, T.A., Belling, J.N., Heizer, P., Tu, Y., Kim, P., Edillo, L., Jonas, S.J., Weiss, P.S., et al. (2019). An

absence of lamin B1 in migrating neurons causes nuclear membrane ruptures and cell death. Proc. Natl. Acad. Sci. USA *116*, 25870–25879.

12. Coffinier, C., Fong, L.G., and Young, S.G. (2010). LINCing lamin B2 to neuronal migration: growing evidence for cell-specific roles of B-type lamins. Nucleus *1*, 407–411.

13. Coffinier, C., Jung, H.J., Nobumori, C., Chang, S., Tu, Y., Barnes, R.H., 2nd, Yoshinaga, Y., de Jong, P.J., Vergnes, L., Reue, K., et al. (2011). Deficiencies in lamin B1 and lamin B2 cause neurodevelopmental defects and distinct nuclear shape abnormalities in neurons. Mol. Biol. Cell *22*, 4683–4693.

14. Young, S.G., Jung, H.J., Coffinier, C., and Fong, L.G. (2012). Understanding the roles of nuclear A- and B-type lamins in brain development. J. Biol. Chem. *287*, 16103–16110.

15. Young, S.G., Jung, H.-J., Lee, J.M., and Fong, L.G. (2014). Nuclear lamins and neurobiology. Mol. Cell. Biol. *34*, 2776–2785.

16. Lee, J.M., Tu, Y., Tatar, A., Wu, D., Nobumori, C., Jung, H.J., Yoshinaga, Y., Coffinier, C., de Jong, P.J., Fong, L.G., and Young, S.G. (2014). Reciprocal knock-in mice to investigate the functional redundancy of lamin B1 and lamin B2. Mol. Biol. Cell *25*, 1666–1675.

17. Lee, J.M., Jung, H.J., Fong, L.G., and Young, S.G. (2014). Do lamin B1 and lamin B2 have redundant functions? Nucleus *5*, 287–292.

18. Giacomini, C., Mahajani, S., Ruffilli, R., Marotta, R., and Gasparini, L. (2016). Lamin B1 protein is required for dendrite development in primary mouse cortical neurons. Mol. Biol. Cell *27*, 35–47.

19. Mahajani, S., Giacomini, C., Marinaro, F., De Pietri Tonelli, D., Contestabile, A., and Gasparini, L. (2017). Lamin B1 levels modulate differentiation into neurons during embryonic corticogenesis. Sci. Rep. *7*, 4897.

20. Gigante, C.M., Dibattista, M., Dong, F.N., Zheng, X., Yue, S., Young, S.G., Reisert, J., Zheng, Y., and Zhao, H. (2017). Lamin B1 is required for mature neuron-specific gene expression during olfactory sensory neuron differentiation. Nat. Commun. *8*, 15098.

21. Yang, S.H., Jung, H.J., Coffinier, C., Fong, L.G., and Young, S.G. (2011). Are B-type lamins essential in all mammalian cells? Nucleus *2*, 562–569.

22. Padiath, Q.S., Saigoh, K., Schiffmann, R., Asahara, H., Yamada, T., Koeppen, A., Hogan, K., Ptácek, L.J., and Fu, Y.-H. (2006). Lamin B1 duplications cause autosomal dominant leukodystrophy. Nat. Genet. *38*, 1114–1123.

23. Pedroso, J.L., Munford, V., Bastos, A.U., Castro, L.P., Marussi, V.H.R., Silva, G.S., Arita, J.H., Menck, C.F.M., and Barsottini, O.G. (2017). LMNB1 mutation causes cerebellar involvement and a genome instability defect. J. Neurol. Sci. *379*, 249–252.

24. Sobreira, N., Schiettecatte, F., Valle, D., and Hamosh, A. (2015). GeneMatcher: a matching tool for connecting investigators with an interest in the same gene. Hum. Mutat. *36*, 928–930.

25. Anna, A., and Monika, G. (2018). Splicing mutations in human genetic disorders: examples, detection, and confirmation. J. Appl. Genet. *59*, 253–268.

26. Reese, M.G., Eeckman, F.H., Kulp, D., and Haussler, D. (1997). Improved splice site detection in Genie. J. Comput. Biol. *4*, 311–323.

27. Wang, M., and Marín, A. (2006). Characterization and prediction of alternative splice sites. Gene *366*, 219–227.

28. Tsai, M.Y., Wang, S., Heidinger, J.M., Shumaker, D.K., Adam, S.A., Goldman, R.D., and Zheng, Y. (2006). A mitotic lamin B matrix induced by RanGTP required for spindle assembly. Science *311*, 1887–1893.